JOURNAL OF OPTOELECTRONICS AND ADVANCED MATERIALS Vol. 22, No. 3-4, March – April 2020, p. 136 - 142

Nanostructured silicon based antireflective layers for thermal infrared optical components

R. REBIGAN[a], M. KUSKO[a,*], G. SOROHAN[b], D. URSU[b], M. GEORGESCU[b], O. TUTUNARU[a], R. TUDOR[a], R. TOMESCU[a], D. CRISTEA[a], C. KUSKO[a,*]

[a]*National Institute for R&D in Microtechnologies – IMT Bucharest, 126 A Erou Iancu Nicolae, Bucharest Romania*

[b]*ProOptica S.A Bucharest Romania*

We investigated the antireflective properties of nanostructured silicon layers fabricated by metal – assisted wet silicon etching. The morphological characterizations reveal that the nanostructured surface consists of holes with diameters in the range of several tens of nanometers, presenting filling factors of 0.50 and with depths in the range of 1 – 1.3 µm. The structures configuring the silicon surface have features much smaller than that of the wavelength of the radiation in the mid – infrared spectrum domain such that the layer can be regarded as homogeneous. The FTIR spectroscopy determinations show that this layer is antireflective over a broad range of infrared wavelengths realizing efficient AR coatings for infrared optical components made on silicon.

(Received September 4, 2019; accepted April 9, 2020)

Keywords: Antireflecting layers, Nanostructured silicon, Infrared optics, Metal assisted chemical etching

1. Introduction

Optical components for thermal imaging systems operate in the mid - infrared spectral domain and are generally fabricated from low infrared absorption materials such as silicon, germanium or zinc selenide [1]. They have high refractive indices in the infrared spectrum; for instance at the wavelength λ=10 µm n_{Si}=3.41, n_{Ge}=4 and n_{ZnSe}=2.4. This fact gives a high optical power for thin lenses manufactured from these materials, but on the other hand, the high contrast of the refractive index of the lens and the one of the surrounding medium such as air or vacuum yields a high interfacial reflection coefficient $r=(n-1)/(n+1)$, a high reflectance $R=|r|^2$ and implicitly a lower transmittance $T=1-R$. For instance, in the case of silicon these values are: r=0.54, R=0.30 and, respectively, T=0.7. Moreover, by accounting for multiple reflections on the two interfaces of an optical component, one obtains a combined reflectance $Rt=2R/(1+R)$ of 0.45 and a combined transmittance of 0.55. These reflection losses are inacceptable for any performant optical system operating in infrared such that the mitigating solution of the antireflective (AR) coatings applied on the interfaces of infrared components is mandatory.

There are several modalities of realizing the antireflective coatings. The most common one is to deposit on the interfaces of the optical components one or more thin films of materials with refractive indices and thicknesses engineered in such a way to reduce the overall reflection coefficients for a certain spectral domain [2]. In the case of a single layer, the cancelation of the reflectivity is attained for a single wavelength, the conditions being that the refractive index n_{AR} of the AR film is the geometrical average of the refractive index n_{sub} of the substrate and the one of the air n_{air} $n^2_{AR}=n_{sub}n_{air}$ and the thickness of the layer is a quarter wavelength. For attaining broadband zero reflectivity, more complex structures such as multilayers or gradient refractive index configurations are to be applied [3]. This modality of realizing AR configurations is technologically mature albeit it requires only certain types of materials with appropriate refractive indices for fulfilling the AR conditions and also a high accuracy for the thicknesses of the deposited layers.

An alternative method to obtain AR layers is to nanopattern the surface of the optical component in order to give it a porosity that decreases its refractive index until it fulfils the matching conditions for antireflectivity [3,4]. An important condition for the nanostructured surface is that the size of the surface's individual features need to be much smaller than the wavelength of the incident radiation such that the AR layer could be regarded as homogeneous avoiding in this way the surface scattering. The nanopatterned surface can be described by an effective model approximation where the effective refractive index is determined by the interplay of the phases (air and substrate) the AR is consisting of, and the filling factor [5]. In this case, the refractive index of the porous material is given by the relation

$$\frac{n_p^2-1}{n^2-1} = 1 - f, \quad (1)$$

where f is the filling factor, n_p is the refractive index of the configured surface and n is the refractive index of the substrate [4]. In general, nanostructured surfaces were applied as AR layers in photovoltaic devices in order to increase their overall efficiencies [6-8] in the visible and near infrared parts of the optical spectrum. Nevertheless, there were studies of the AR effect of the nanostructured configurations in the mid-infrared, far-infrared and THz

frequencies where it was demonstrated a dramatic reduction in the reflectivity [9].

In this article, we configured a nanostructured surface on a silicon substrate by a modified metal assisted chemical etching (MACE) [10] using a discontinuous silver mask layer of several nanometer thickness. We selected this technique for its low cost and for the possibility to cover large areas, such that it can be used for fabricating low cost AR coatings for silicon infrared optical components.

The resulting sub-wavelength structures (SWS) consist of holes with the diameters of approximately 50 – 60 nm, with their depths in the range of 1-1.3 µm and an overall filling factor of approximately 50%. The process was optimized in order to obtain the geometrical parameters of the AR film such that overall reduction of the silicon reflectivity in the mid-infrared should be attained. The nanostructured AR was realized on an interface of a silicon wafer with both sides polished in order to avoid the scattering on the other interface. In order to evaluate the reduction in the reflectance, and respectively the improvement in the transmittance we performed FTIR measurements in both reflection and transmission mode in the spectral range 5 – 20 µm. As a reference, we performed these measurements on a double side polished silicon wafer. By fitting the experimental data with the reflection calculations where we took into account the multiple reflections we obtained the attenuation factor and, respectively, the imaginary part of the refractive index of the silicon. The experimental results show that the SWS based AR layer induces a broadband overall increase in the transmittance of the sample. While this increase indicates that the SWS acts as an AR layer we did not observe any interference minima and maxima. This fact suggests that the SWS based AR should be regarded as an incoherent or a partially coherent layer. We have qualitatively fitted the experimental data with reflectivity calculations taking into account the absorbance determined from the double side polished silicon wafer and considering a series of geometrical parameters of the AR SWS layer in terms of SWS height and filling factor. We observed a good agreement between experiment and calculation in the longer part of infrared spectrum 12 – 20 µm, while in the shorter part of the spectrum 5 – 12 µm the theoretical calculations reveal interference minima and maxima in contrast with the experimental results. This suggest that the reflectance and transmittance can be interpreted as an average over different heights and filing factors of the AR SWS layer.

2. Experimental

Metal-assisted wet silicon etching is a cheap method for silicon nanowires (Si NWs) synthesis [11–15]. This method uses an etching solution of HF (molar concentration 5M), and H_2O_2 (molar concentration 0,44 M) and a metallic discontinuous layer. In this type of metal-assisted silicon etching process, the metal (silver) catalyzes Si oxidation by H_2O_2 and then SiO_2, selectively formed where metal and Si are in contact, is etched by HF. This process is a modified metal-assisted wet etching (MACE), exploiting the replacement of the salt ($AgNO_3$) with a metallic discontinuous thin film (Ag of several nanometers thickness).

The thin metallic discontinuous layer injects holes into the underlying Si substrate, and here Si oxidation occurs, while the presence of HF determines SiO_2 removal and the sinking of the metal into silicon, hence it produces silicon etching. Therefore, SWS formation occurs in the regions which are not covered by the metal [15]. This etching process has two relevant advantages: no residues due to the etching process are present and better control over the Si NWs structural properties is obtained.

A thin discontinuous metallic thin layer of silver has been deposited using e-beam evaporation NEVA equipment on a double side polished silicon wafer. The several nm thickness Ag layer is characterized by a peculiar morphology, which leaves uncovered a relevant fraction of the Si surface. Within this thickness range, the morphology of the metallic layer and the etching solution determine the formation of NWs having an extremely small diameter (tens of nanometers), and different heights depending on etching time. The Ag deposition parameters were: i) deposition chamber pressure: $3x10^{-6}$ torr, ii) electron beam current: I=120mA iii) deposition time: t=180s corresponding to deposition rate of 0.3-0.5 Å/s. The deposition rate has been monitored in real time using a quartz crystal.

Surface morphology and thickness of Ag layer as well as Si SWS were evaluated by Field Emission Gun Scanning Electron Microscope (FEG-SEM) with ultra-high resolution - FEI Nova NanoSEM 630. In order to evaluate the fill factor in the SEM images we used the software ImageJ to calculate the coverage percentage by estimating the area covered by pores/Ag particles and the area occurred by Si.

To evaluate the efficient Ag removal after SWS fabrication we have used the element energy dispersive spectroscopy (EDS) system (Smart Insight AMETEK – EDAX Smart Insight).

In Fig. 1 are presented the SEM and AFM images of Ag discontinuous metallic layer as deposited. The metallic particles are disordered and present different sizes – with diameters in the order of magnitude of tens of nanometers.

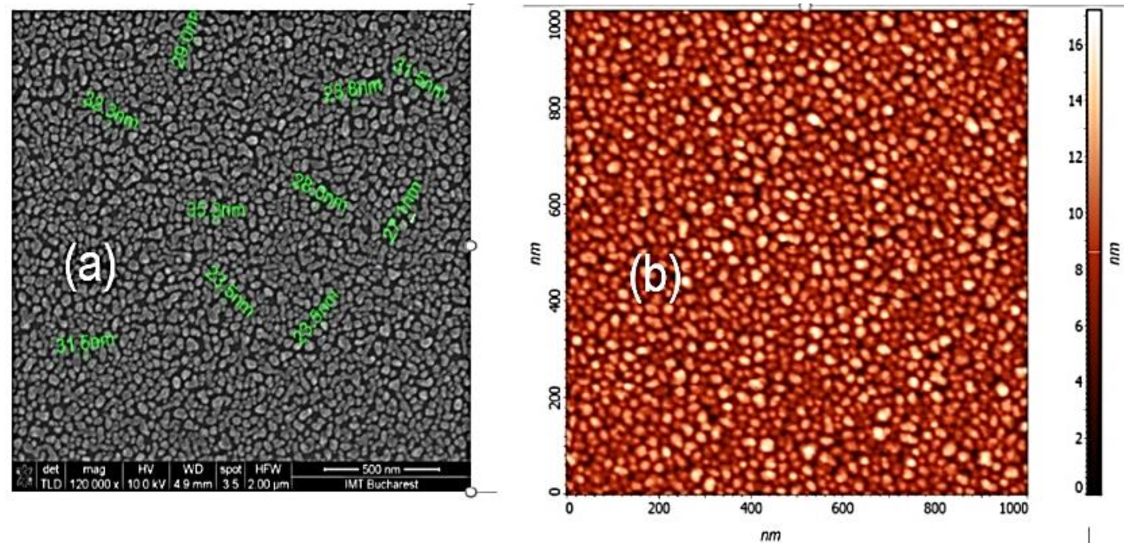

Fig. 1. (a) SEM images (top view) of the Ag discontinuous metallic layer as deposited (scale bar 1 µm) (b) AFM 2D image of the Ag discontinuous layer as deposited (color online)

Therefore, in order to control the SWS formation, the metallic discontinuous layer has been thermally annealed at 300ºC for 30 min on a hotplate. Due to the thermal annealing, Ag particles were ordered exhibiting a spherical form, as seen in Fig. 2 which shows the SEM and AFM correlated measurements.

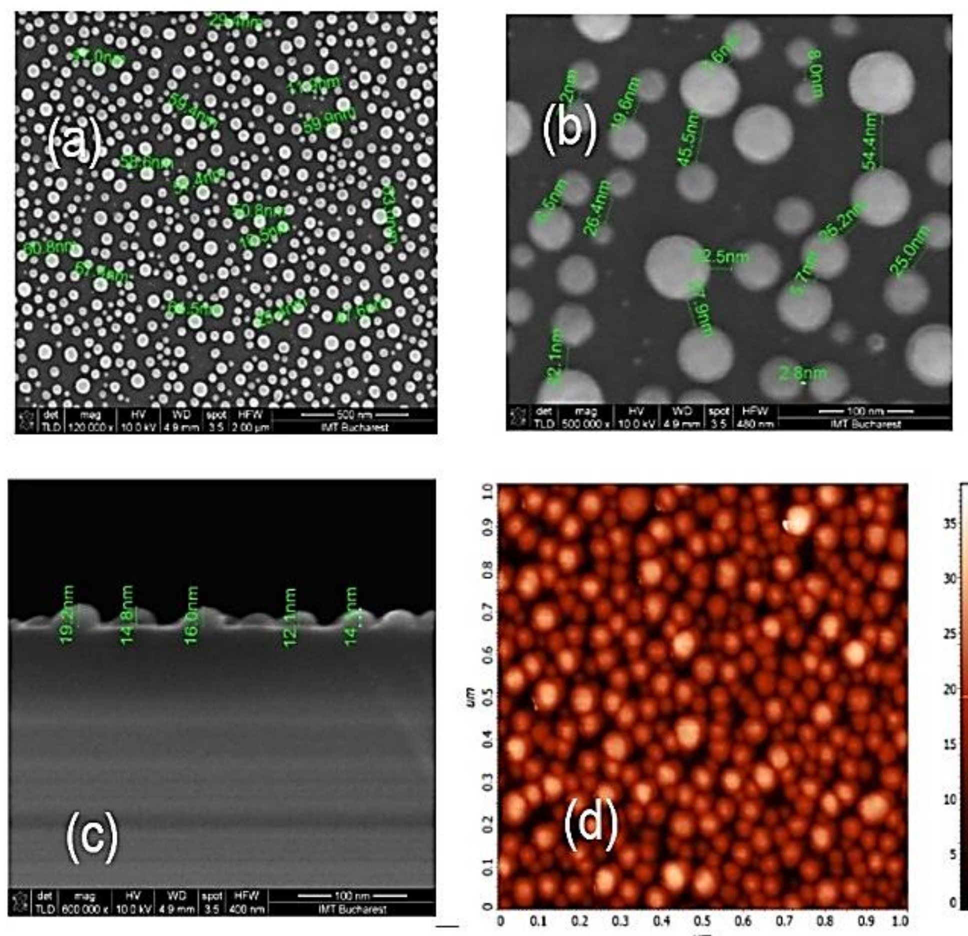

Fig. 2. SEM images of Ag discontinuous layer after thermal annealing: (a) and (b) top view images of the sample at two different magnifications, (c) measured size particles (cross section image) and (d) AFM image of Ag layer (color online)

For configuring the Si SWS, two samples consisting of silicon double side polished wafers, p (100), resistivity of 1 – 10 Ω cm were etched for 4 and 6 minutes, respectively, using HF (5M):H_2O_2 (0.44M) solution through the thermally discontinuous annealed metallic Ag layer with thickness < 10 nm. The heights of the SWS are less than 1 µm for the one etched for 4 minutes and 1.3 µm the one etched for 6 minutes. The later structures are displayed in Fig. 3 where SEM images show the top view of the layer (a) as well as the cross section view with the height measurements only in the case of the second sample.

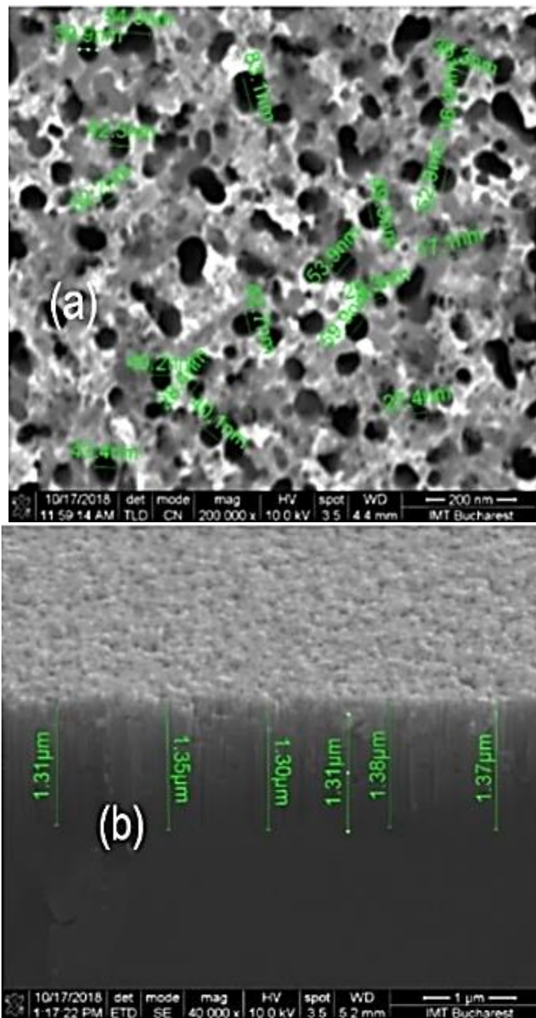

Fig. 3. SEM image of SWS: (a) top view image with size measurements; (b) cross section image showing SWS measured heights (color online)

After SiNW etching, thin Ag layer has been chemically removed using ammonia solution (25%) for 20 s for the oxidized silver, and I_2 + KI solution respectively for the silver removal itself (1 minute in ultrasound bath).

For the evaluation of fill factor in SEM images we used the software ImageJ to calculate the coverage percentage by estimating the area covered by pores/Ag particles and the area of Si. From the SEM images of Ag layer as deposited and after thermal annealing, SiNW etched for 4 and 6 minutes we have extracted the fill factor using the same magnification in SEM images (Tabel 1).

Table 1. Fill factor for the two samples presenting a layer of Si based SWS were the etching times are 4 minutes and 6 minutes

Sample	*Fill factor (%)*
Ag layer as deposited	*78*
Ag layer thermally annealed	*47*
SiNW etched for 4 minutes	*47*
SiNW etched for 6 minutes	*49*

While Ag coverage decreases with thermal annealing, remaining Si resulting from SWS etching has approximately the same coverage on sample area, meaning that the etching depth does not modify the fill factor on SWS samples. Efficient Ag removal after SWS fabrication was investigated using EDX spectroscopy (by energy dispersion). As reference, a sample featuring only the thin Ag discontinuous layer, before silicon etching was used. In the X ray energy dispersion spectroscopy, the presence of silver (Ag) is observed at the specific EDX peak of 2,984 keV, while Si at the specific peak specific of 1,740 keV confirming the presence of Ag and Si as it can be seen from Fig. 4 (a). The two samples with the different etching times featuring SWS were investigated by EDX spectroscopy after Ag chemical removal, on different areas, to identify the presence or the absence of residual Ag particles. Fig. 4 (b) shows the EDX spectra performed in several selected areas of the first sample featuring SWS revealing that there are no Ag peaks which indicates the complete removal of the silver after SWS etching.

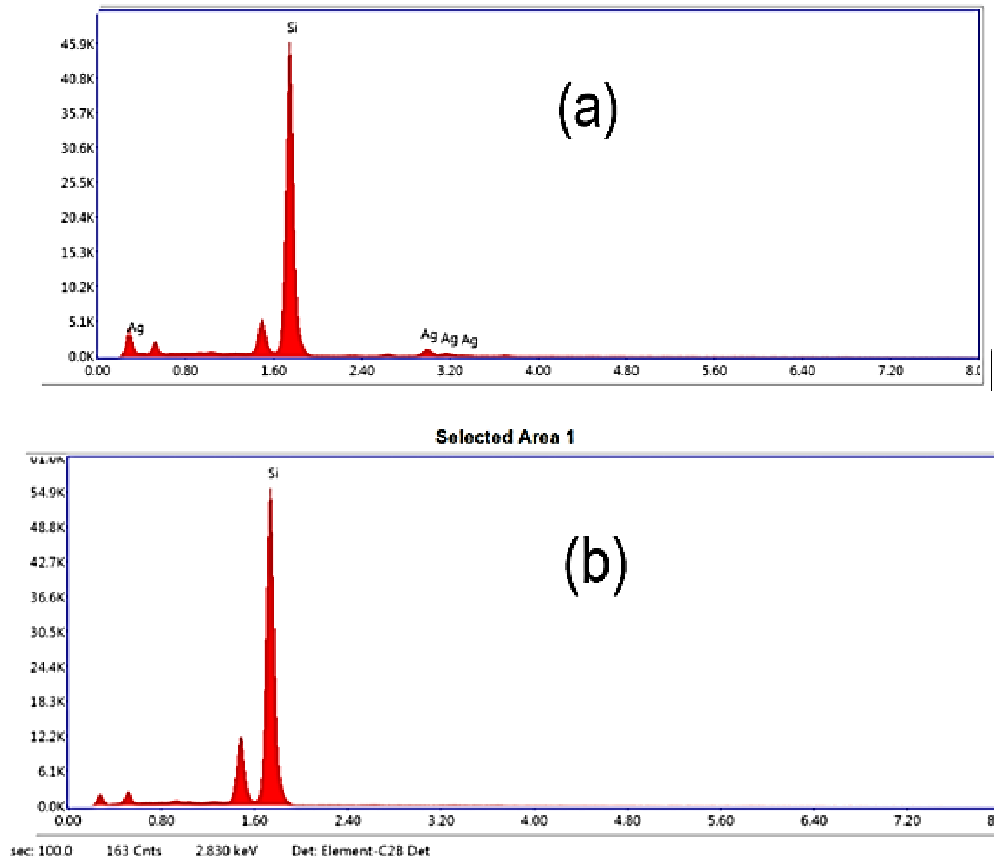

Fig. 4. EDX spectra of (a) unetched sample featuring Ag discontinuous layer on silicon substrate, (b) etched sample after Ag removal (color online)

3. Results

The reflectance and transmittance were measured with a FTIR spectrometer VERTEX 80/80v Bruker Optics in the mid – infrared spectral domain in the range of 5 – 20 µm wavelengths. For the reflectance measurement, the reference was a gold mirror while for the transmittance the reference was vacuum. The reflectance and transmittance measurements for a double side polished silicon wafer (red lines) and the ones for the silicon wafer configured with SWS AR (black line) are displayed in Fig. 5 and Fig. 6 respectively. It can be seen that in comparison with double side polished silicon wafers, the reflectance of the SWS AR sample presents a significant constant decrease over the entire investigated spectral range. At the same time the transmittance presents a constant increase demonstrating the influence of the SWS AR layer. The absence of interference minima and maxima which are characteristic to a single wavelength AR layer indicates that either the layer can be described as incoherent [16], or that the reflection can be considered as an average over a distribution of heights and porosities of the nanostructured silicon.

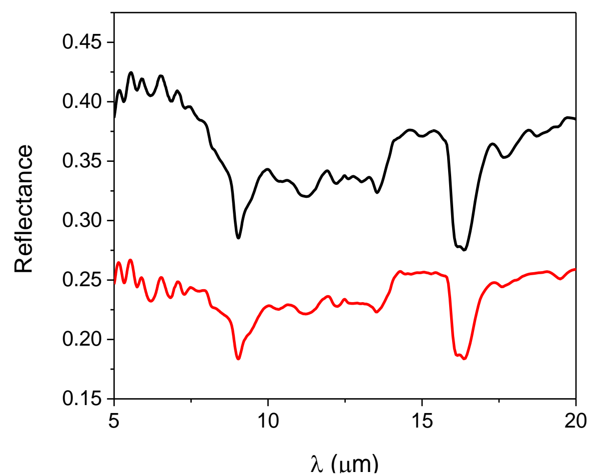

Fig. 5. Reflectance spectra for the double side polished silicon wafer (black line) and for the silicon wafer with SWS AR (red line) (color online)

In order to test the latter assumption, we performed reflectivity calculations for a series of parameters of the AR layer such as the heights of the SWS, and the filing factor which according to eq. 1 determines the effective refractive index.

For that, from the transmittance spectra of the double side polished silicon wafers we firstly evaluated the attenuation of silicon in the mid infrared spectral domain, and, respectively, the imaginary part of the silicon refractive index. In Fig. 7 we show again the experimental transmittance (Fig .6) displayed, in this case with black empty circles fitted with the calculated transmittance displayed with red solid line. We took into account the multiple reflections occurring on both interfaces of the double side polished silicon wafers. Since the thickness of the wafer (525 μm) is much larger than the coherence length in the mid infrared we did neglected the interference effects summing the field intensities and not the amplitudes. The attenuation was considered by choosing an imaginary part of the refractive index which is given by the phonons contribution in the infrared [17] shown in Fig. 8.

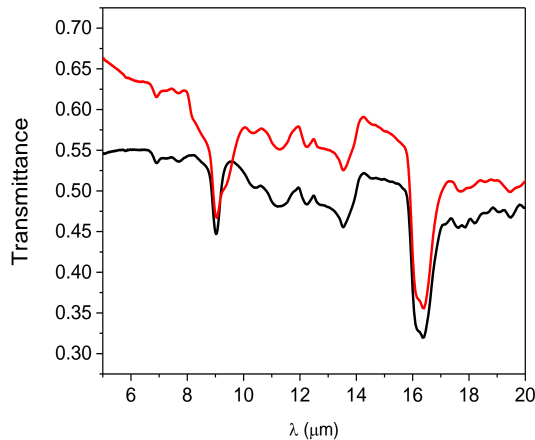

Fig. 6. Transmittance spectra for the double side polished silicon wafer (black line) and for the silicon wafer with SWS AR (red line) (color online)

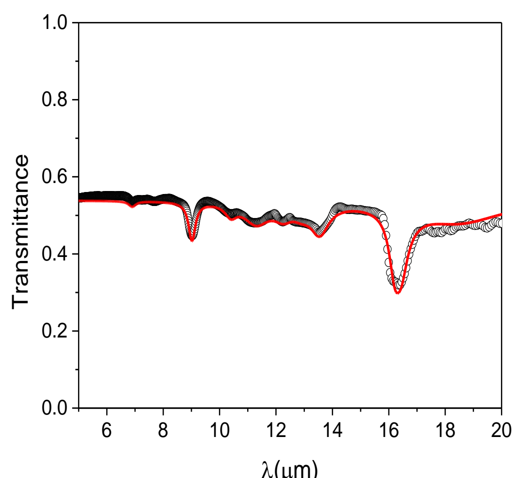

Fig. 7. Experimental transmittance spectra for the double side polished silicon wafer (black empty circles) and the calculated one (red line) (color online)

Then, we performed transmittance calculations for a series of geometrical and material parameters describing the AR SWS layer. Specifically, we considered three effective refractive indices n=1.8, n=2.2 and n=2.5 for the hole depths of 1 μm and 1.3 μm. The transmittance calculations for the AR layer are shown in Fig. 9 plotted together with the experimental data (black empty circles). In these calculations both the attenuation as well as the multiple reflections were taken into account.

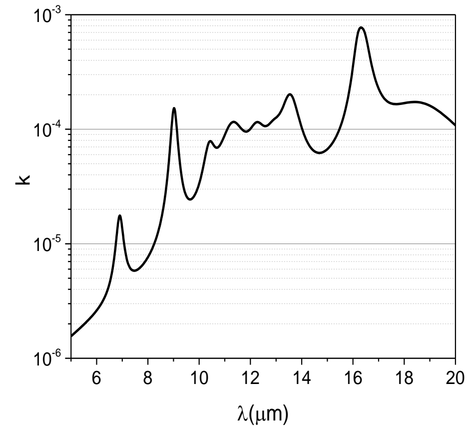

Fig. 8. Imaginary part of the silicon refractive index determined from the experimental data

It can be seen that while the longer part of the infrared spectrum can be fitted semi-quantitatively by the parameters n=2.2 and d=1.0 μm, at shorter wavelengths the appearance of the interference minima and maxima prevent even a qualitatively fit. On the other hand, the porous layer can be regarded as a distribution of holes with various heights and diameters, therefore the total reflectance and transmittance can be regarded as an average over the entire distribution of parameters, as it is indicated by Fig 9.

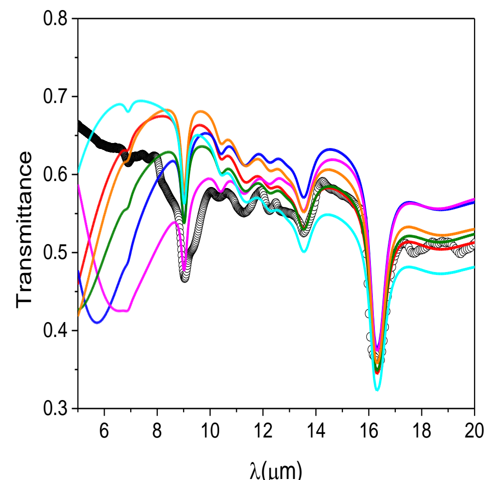

Fig. 9. Theoretical transmittance calculations colored solid line plotted together with the experimental data (black empty circles) for a series of geometrical and material parameters of the SWS AR layer: red n=2.2, d=1.0 μm; blue n=2.2, d=1.3 μm; magenta n=2.5, d=1.0 μm; green n=2.5, d=1.3 μm; light blue n=1.8, d=1.0 μm; orange n=1.8, d=1.3 μm (color online)

4. Conclusions

In this article we investigated the nano-configuration of the silicon surface with a layer consisting of holes with diameters in the range of tens of nanometers and depths of 1 -1.5 μm using metal assisted chemical etching technique. Performed FTIR measurements reveal a significant decrease in the reflectivity covering the entire range of the investigated infrared spectrum. At the wavelengths where the silicon absorption can be neglected, λ=5 μm and λ=20 μm the reflectance decreases from 0.40 to 0.25. The low cost of the metal assisted chemical etching, the possibility to nano-configure large areas such as entire wafers of silicon, as well as broadband antireflectivity properties, indicate that this method is suitable for realizing AR coatings for infrared optical components made on silicon.

Acknowledgements

This work was supported by POC Project TGE – PLAT, Contract no. 77/08.09.2016, subsidiary contract C772D, "High quality image forming optical system with optical diffractive elements in LWIR spectral range, for multi – sensing systems – SOFID".

Thanks

Special thanks to our colleagues Phys. Raluca Gavrila for providing AFM measurements and Dr. Antonio Radoi for FTIR spectroscopy transmission measurements.

References

[1] A. Mann, Infrared Optics and Zoom Lenses, Second edition, SPIE Press, (2009).
[2] Ph. W. Baumeister, Optical Coating Technology, SPIE Press (2004).
[3] S. Chattopadhyay, Y. F. Huang, Y. J. Jen, A. Ganguly, K. H. Chen, L. C. Chen, Materials Science and Engineering R **69**, 1 (2010).
[4] B. Yoldas, Applied Optics **9**, 1425 (1980).
[5] D. A. G. Bruggeman, Annalen der Physik **416**, 636 (1935).
[6] J. Y. Chen, W.-L. Chang, C. K. Huang, K. W. Sun, Opt. Expr. **19**, 14411 (2011).
[7] Yunfeng Li, Junhu Zhang, Bai Yang, Nano Today **5**, 117 (2010).
[8] Mahdi Motamedi, Felipe Crisostomo, Yin Yao, Sajjad S Mofarah, Wen-Fan Chen, Pramod Koshy, Robert A. Taylor, Journal of Physics D: Applied Physics **52**, 315501 (2019).
[9] Yi-Fan Huang et al., Nature Nanotechnology **2**, 770 (2007).
[10] Hee Han, Zhipeng Huang, Woo Lee, Nano Today **9**, 271 (2014).
[11] K. Q. Peng, Y. Wu, H. Fang, X. Y. Zhong, Y. Xu, J. Zhu, Angew. Chem. Int. Edn **44**, 2737 (2005).
[12] Z. P. Huang, T. Shimizu, S. Senz, Z Zhang, N. Geyer, U. Gosele, J. Phys. Chem. **C 114**, 10683 (2010).
[13] K. Peng, Y. Xu, Y. Wu, Y. Yan, S. T. Lee, J. Zhu, Small **1**, 1062 (2005).
[14] L. Lin, S. Guo, X. Sun, J. Feng, Y. Wang, Nanoscale Res. Lett. **5**, 1822 (2010).
[15] A. Irrera, P. Artoni, F. Iacona, E. F. Pecora, G. Franzò, M. Galli, B. Fazio, S. Boninelli, F. Priolo, Nanotechnology **23**(7), 075204 (2012).
[16] R. Santbergen, A. H. M. Smets, M. Zeman, Opt. Expr. **21**, A263 (2013).
[17] D. Chandler-Horowitz, P. M. Amirtharaj, J. Appl. Phys. **97**, 123526 (2005).

*Corresponding author: cristian.kusko@imt.ro